

## UNVEILING OBSCURED ACCRETION IN THE CHANDRA DEEP FIELD–SOUTH

F. FIORE,<sup>1</sup> A. GRAZIAN,<sup>1</sup> P. SANTINI,<sup>1,2</sup> S. PUC CETTI,<sup>3</sup> M. BRUSA,<sup>4</sup> C. FERUGLIO,<sup>1</sup> A. FONTANA,<sup>1</sup> E. GIALLONGO,<sup>1</sup>  
A. COMASTRI,<sup>5</sup> C. GRUPPIONI,<sup>5</sup> F. POZZI,<sup>6</sup> G. ZAMORANI,<sup>5</sup> AND C. VIGNALI<sup>6</sup>

Received 2007 April 23; accepted 2007 September 9

### ABSTRACT

We make use of deep *HST*, *VLT*, *Spitzer*, and *Chandra* data on the Chandra Deep Field–South to constrain the number of Compton-thick AGNs in this field. We show that sources with high 24  $\mu\text{m}$ –to–optical flux ratios and red colors form a distinct source population, and that their infrared luminosity is dominated by AGN emission. Analysis of the X-ray properties of these extreme sources shows that most of them ( $80\% \pm 15\%$ ) are indeed likely to be highly obscured, Compton-thick AGNs. The number of infrared-selected, Compton-thick AGNs with 5.8  $\mu\text{m}$  luminosity higher than  $10^{44.2}$  ergs  $\text{s}^{-1}$  turns out to be similar to that of X-ray-selected, unobscured, and moderately obscured AGNs with 2–10 keV luminosity higher than  $10^{43}$  ergs  $\text{s}^{-1}$  in the redshift bin 1.2–2.6. This “factor of 2” source population is exactly what is needed to solve the discrepancies between model predictions and X-ray AGN selection.

*Subject headings:* galaxies: active — galaxies: high-redshift — X-rays: diffuse background

*Online material:* color figures

### 1. INTRODUCTION

Active galactic nuclei (AGNs) are not only witnesses of the phases of galaxy formation and/or assembly but are most likely among the leading actors. Indeed, three seminal discoveries indicate tight links and feedbacks between supermassive black holes (SMBHs), nuclear activity, and galaxy evolution. The first is the discovery of SMBHs in the center of most nearby bulge-dominated galaxies and the tight correlation between their masses and galaxy bulge properties (Gebhardt et al. 2000; Ferrarese & Merritt 2000; Marconi & Hunt 2003 and references therein). The second is that the growth of SMBHs is mostly due to accretion of matter during their active phases, and therefore that most bulge galaxies passed a phase of strong nuclear activity (Soltan 1982; Marconi et al. 2004). The third is that the evolution of AGNs is luminosity-dependent, with lower luminosity AGNs peaking at a redshift lower than luminous QSOs (Hasinger 2003; Hasinger et al. 2005; Fiore et al. 2003; Ueda et al. 2003; La Franca et al. 2005; Brandt & Hasinger 2005; Bongiorno et al. 2007), a bimodal behavior recalling the evolution of star-forming galaxies and of massive spheroids (Cowie et al. 1996; Franceschini et al. 1999; De Lucia et al. 2006). All three discoveries imply that obtaining a complete census of accreting SMBHs through the cosmic epochs and constraining accretion efficiency and feedbacks are crucial steps toward the understanding of Galaxy formation and evolution.

The first attempts to constrain models for the formation and evolution of structure in the universe using the evolving optical and X-ray AGN luminosity functions have been presented by Granato et al. (2001, 2004), Di Matteo et al. (2005), and Menci et al. (2004, 2005). In particular, the Menci et al. model links the evolution of the galaxies in the hierarchical clustering scenarios with the changing accretion rates of cold gas onto the central SMBH that powers the QSO (Cavaliere & Vittorini 2000). The results of this model

were encouraging, in the sense that it predicts a trend of lower luminosity AGNs peaking at increasingly lower redshift, as observed. However, from a quantitative point of view, the model overpredicts by a factor of about 2 the space density of low-to-intermediate luminosity (Seyfert-like) AGNs at  $z = 1.5$ – $2.5$  with respect to present X-ray observations. Furthermore, Marconi et al. (2004) derived a SMBH mass function from the X-ray-selected AGN luminosity functions (e.g., La Franca et al. 2005) that falls short by a factor of about 2 of the “relic” SMBH mass function, evaluated using the  $M_{\text{BH}}\text{-}\sigma_V/M_{\text{BH}}\text{-}M_B$  relationships and the local bulge’s luminosity function. The most likely explanation for both discrepancies is that present X-ray surveys, although very efficient for probing unobscured and moderately obscured AGNs (with column densities up to a few  $\times 10^{23}$   $\text{cm}^{-2}$ , the so-called Compton-thin AGNs), miss most of the very highly obscured but still strongly accreting objects, the so-called Compton-thick AGNs, with a column density  $N_{\text{H}} \gtrsim 10^{24}$   $\text{cm}^{-2}$  (see Comastri 2004). Indeed, only a handful of the faintest sources in the Chandra Deep Fields may be Compton-thick (see La Franca et al. 2005 and Tozzi et al. 2006). So, we still may be viewing just the tip of the iceberg of the highly obscured AGN population. Compton-thick objects may well be more common at high redshift, as suggested on theoretical grounds by Silk & Rees (1998) and Fabian (1999) and on observational grounds by, e.g., Gilli et al. (2001), Worsley et al. (2004, 2006), and La Franca et al. (2005).

Compton-thick AGNs at  $z \gtrsim 1$  can be recovered thanks to the reprocessing of the AGN UV emission in the infrared by selecting sources with AGN luminosities in the mid-infrared and faint near-infrared and optical emission (e.g., Martinez-Sansigre et al. 2005, 2006; Houck et al. 2005; Weedman et al. 2006a, 2006b). We investigate this issue further by making use of the multiwavelength data obtained on the Chandra Deep Field–South (CDFs; Giacconi et al. 2002), one of the fields with the deepest coverage at optical, infrared, and X-ray wavelengths. A  $H_0 = 70$   $\text{km s}^{-1}$   $\text{Mpc}^{-1}$ ,  $\Omega_M = 0.3$ ,  $\Omega_\Lambda = 0.7$  cosmology is adopted throughout.

### 2. DATA SETS AND SAMPLE SELECTION

The selection and spectroscopic identification of complete AGN samples from mid-infrared surveys is a rather difficult task,

<sup>1</sup> INAF—Osservatorio Astronomico di Roma, Via Frascati 33, I-00040 Monteporzio, Italy.

<sup>2</sup> Università di Roma La Sapienza, Rome, Italy.

<sup>3</sup> ASI Science Data Center, Via Galileo Galilei, 00044 Frascati, Italy.

<sup>4</sup> Max-Planck-Institut für extraterrestrische Physik, Giessenbachstrasse 1, D-85748 Garching bei München, Germany.

<sup>5</sup> INAF—Osservatorio Astronomico di Bologna, Via Ranzani 1, Bologna, Italy.

<sup>6</sup> Università di Bologna, Via Ranzani 1, Bologna, Italy.

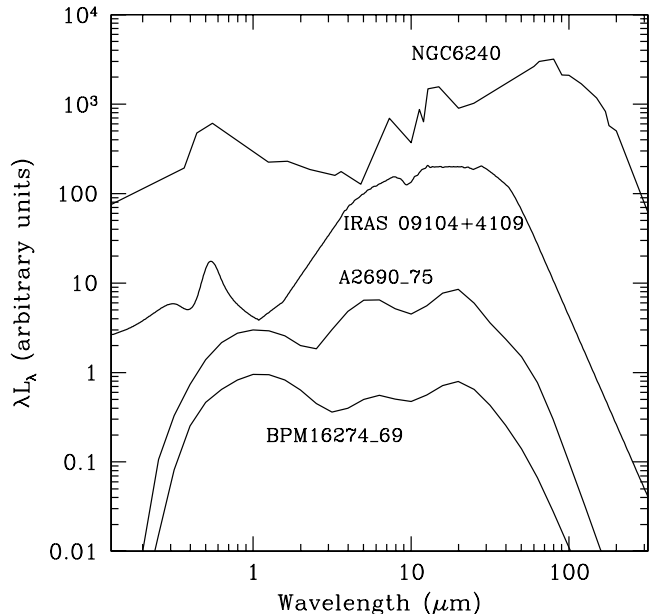


FIG. 1.—  $\lambda L_\lambda$  SEDs of the four additional templates of sources hosting highly obscured AGNs used in this work. *Top to bottom*: NGC 6240, IRAS 09104+41091, HELLAS2XMM A2690\_75, and BPM 16274\_69.

because AGNs make up only a small fraction of the full mid-infrared source population. Using *Spitzer* IRAC colors results in samples significantly contaminated by star-forming galaxies (e.g., Lacy et al. 2004; Alonso-Herrero et al. 2006; Barmby et al. 2006; Polletta et al. 2006). Comparing the global observed spectral energy distribution (SED) to AGN and galaxy templates proved to be more efficient in selecting AGN samples (Polletta et al. 2006, 2007). However, it is very difficult to assess the completeness of these samples given all the complex selection effects. Furthermore, many obscured AGNs may still be missed by this technique.

We adopt in this paper a somewhat different approach. We do not pretend to select *all* AGNs through optical and infrared photometry. As explained before, X-rays are much more efficient in selecting unobscured (i.e., broad-line) and moderately obscured AGNs. We concentrate our efforts on highly obscured AGNs only, and we limit our analysis to the high infrared luminosity AGN population. The driving consideration is that differences between nuclear and star formation emission are emphasized, comparing the observed SEDs with galaxy templates over a range as broad as possible (also see Martinez-Sansigre et al. 2005, 2006; Houck et al. 2005; Weedman et al. 2006a, 2006b; Magliocchetti et al. 2007). Our primary objective here is to validate our obscured AGN selection criteria and assess the magnitude of the corresponding selection effects using a careful analysis of the deep X-ray data available on the CDFS.

### 2.1. The GOODS-MUSIC Catalog

In this paper we use the latest version of the GOODS-MUSIC catalog (Grazian et al. 2006). We limit the analysis to the region fully covered by deep VLT/ISAAC near-infrared photometry ( $143.2 \text{ arcmin}^2$ ) and to the sources with MIPS  $24 \mu\text{m}$  fluxes  $F(24 \mu\text{m}) > 40 \mu\text{Jy}$  (1729 sources). We obtained  $24 \mu\text{m}$  fluxes for all objects in the catalog following the procedures described in De Santis et al. (2007).

The published version of the catalog contains  $z$ -band and  $K$ -band selected sources in the GOODS-South area. The revised version of the catalog used in this work includes 46 objects that are detected only in the  $4.5 \mu\text{m}$  band, i.e., their  $z$  and  $K$  magnitudes

are below the chosen detection threshold. Only four of these sources do not have counterparts in the optical and/or near-infrared images. At the flux limits adopted here, we do not detect any objects at  $24 \mu\text{m}$  that are not detected at shorter wavelengths. In the following we use Vega magnitudes and cgs fluxes for each entry of the catalog.

The GOODS-MUSIC catalog includes both monochromatic and total infrared luminosities for the sources with reliable spectroscopic or photometric redshifts. Total  $8\text{--}1000 \mu\text{m}$  luminosities were computed by integrating the best-fit galaxy and AGN templates. Monochromatic luminosities were computed by interpolating the observed SEDs at the rest-frame wavelength of interest. A large (factor of 10–30) systematic uncertainty is associated with the total infrared luminosity that is dominated by the contributions at wavelengths of  $\sim 100\text{--}1000 \mu\text{m}$ , well outside the infrared band used in this paper ( $1\text{--}24 \mu\text{m}$ ). Different models can produce similar fits below  $24 \mu\text{m}$  but give rise to large differences in the total infrared luminosity. This systematic uncertainty is greatly reduced using the monochromatic luminosity at  $5.8 \mu\text{m}$  (see, e.g., Yan et al. 2007), since this wavelength is within the observed band up to  $z \sim 3.2$ . For this reason, in the following we make use of the infrared luminosity at  $5.8 \mu\text{m}$  [ $\lambda L_\lambda(5.8 \mu\text{m})$ ] to characterize the infrared power of the CDFS sources.

### 2.2. Galaxy and AGN Templates

A detailed fitting of the observed SEDs using AGN and galaxy templates was also performed. Templates include passive galaxies, star-forming galaxies, unobscured AGNs, and highly obscured AGNs. Spectral libraries include both empirical templates (Coleman et al. 1980 data sets; Polletta et al. 2007) and synthetic models (Bruzual & Charlot 2003; Fioc & Rocca-Volmerange 1997). We take particular care with the description of highly obscured AGNs. In addition to the templates presented by Polletta et al. (2007), we used four templates of sources hosting highly obscured AGNs (Fig. 1). The NGC 6240 template includes  $U, B, V, J, H, K, IRAS$ , and  $ISO$  photometry. The IRAS 09104+41091 template includes SDSS  $u, g, r, i$ , and  $z$  photometry,  $B, V, R, J, H$ , and  $K$  photometry, *Spitzer* IRAC and MIPS photometry, *Spitzer* IRS spectroscopy, and *IRAS* photometry. For the two HELLAS2XMM sources we use the best-fit SED model in Pozzi et al. (2007). These templates span a range of infrared-to-optical flux ratio significantly broader than the obscured AGN templates used by Polletta et al. (2007).

### 2.3. Photometric Redshifts and SED Fittings

Photometric redshifts were derived by Grazian et al. (2006) by fitting only the part of the SED dominated by the integrated stellar population, i.e.,  $\lambda < 5.5 \mu\text{m}$  (Grazian et al. 2006 and references therein). The synthetic models used are very accurate and complete in the treatment of the star formation history and evolution of the stellar populations and of the dust content of the galaxy and its evolution. However, while dust extinction is easy to account for because it is a line-of-sight effect, dust emission and reprocessing is much more complicated to model, since it depends largely on the assumed geometry and covering fraction. Dust emission was therefore not considered in the models, and, accordingly, the bands above  $5.5 \mu\text{m}$  rest frame are ignored in these fits (see Grazian et al. 2006 for further details). This approach produces robust photometric redshifts [ $\Delta z/(1+z) < 0.05$ ] for passive galaxies, star-forming galaxies, and obscured AGNs, where the nuclear optical and infrared emission is completely blocked or strongly reduced by dust and gas along the line of sight. Unobscured AGNs with power-law SEDs are excluded from this analysis (however, most of them have reliable spectroscopic redshift from Cimatti

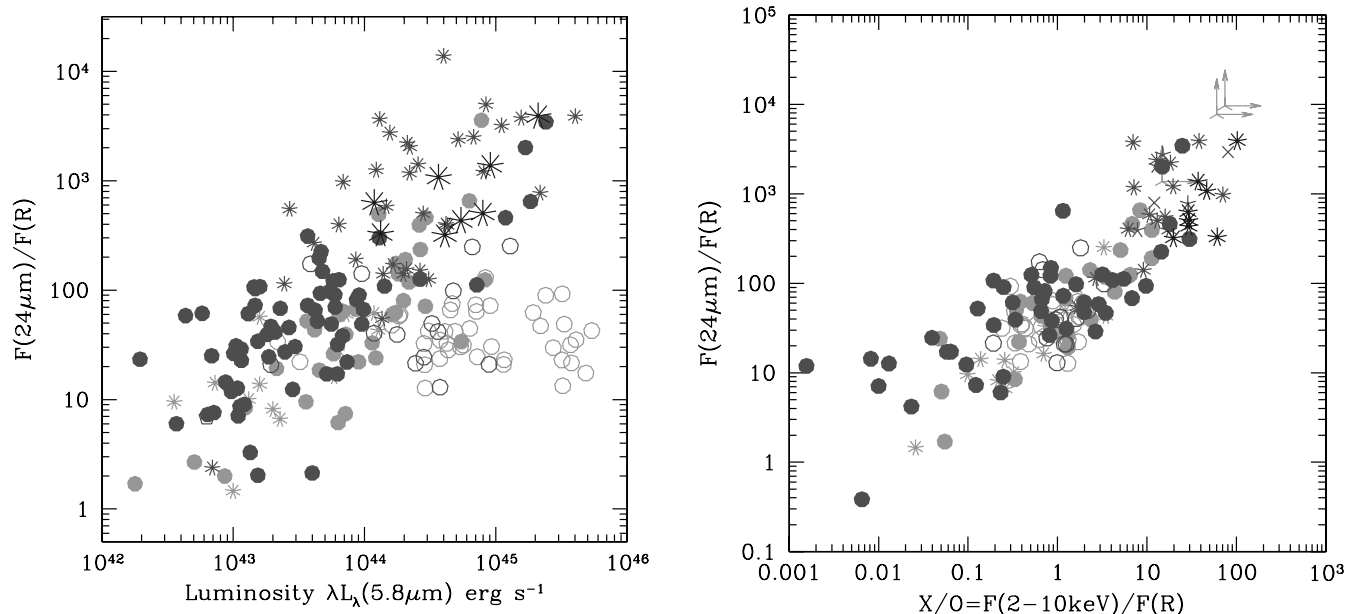


FIG. 2.—*Left:*  $F(24\ \mu\text{m})/F(R)$  as a function of the  $5.8\ \mu\text{m}$  luminosity for three X-ray source samples (GOODS-MUSIC, *black symbols*; ELAIS-S1, *gray symbols*; and HELLAS2XMM, *large asterisks*; Pozzi et al. 2007). Open circles are type 1 AGNs, filled circles are non-type 1 AGNs, and asterisks are photometric redshifts. Note that the  $F(24\ \mu\text{m})/F(R)$  of non-broad-line AGNs is strongly correlated with the luminosity at  $5.8\ \mu\text{m}$ . *Right:*  $F(24\ \mu\text{m})/F(R)$  as a function of the X/O for the same source samples. All symbols are the same as in the left panel; arrows are sources without an optical counterpart. [See the electronic edition of the Journal for a color version of this figure.]

et al. 2002; Szokoly et al. 2004; Le Fevre et al. 2004; Vanzella et al. 2005, 2006; Mignoli et al. 2005).

To characterize each SED we repeated the fit to the observed SED with a library of empirical templates, fixing the redshift to the spectroscopic redshift or, if this is not present, to the photometric redshift obtained as described above. This library includes the 21 templates of passive galaxies, star-forming galaxies, and AGNs by Polletta et al. (2007) and the four templates of systems hosting a highly obscured AGN in Figure 1. The best-fit template and normalization were used to measure monochromatic and total infrared luminosities.

#### 2.4. Optical, Near-Infrared, and Mid-Infrared Color Selection

The longest and shortest wavelengths at which deep photometry is available on the Chandra Deep Fields are the  $24\ \mu\text{m}$  mid-infrared band covered by *Spitzer* MIPS and the optical bands covered by the *HST* Advanced Camera for Surveys (ACS). The  $24\ \mu\text{m}$  sources with faint optical counterparts must be either luminous AGNs whose optical nuclear emission is blocked by dust and gas or powerful dusty starburst galaxies. The mid-infrared-to-optical flux ratio<sup>7</sup> can therefore be considered a rough estimator of obscured activity (both nuclear and star formation) in galaxies.

Figure 2 shows  $F(24\ \mu\text{m})/F(R)$  as a function of  $\lambda L_\lambda(5.8\ \mu\text{m})$  for three samples of X-ray sources. Unobscured AGNs (Fig. 2, *open symbols*) have  $F(24\ \mu\text{m})/F(R)$  in the range 10–200, uncorrelated with  $\lambda L_\lambda(5.8\ \mu\text{m})$ , as expected because the nuclear emission dominates both optical and mid-infrared wavelengths. Conversely, obscured AGNs (*filled symbols*) have  $F(24\ \mu\text{m})/F(R)$  spanning a broader range and fairly correlated with  $\lambda L_\lambda(5.8\ \mu\text{m})$ . This behavior resembles that of moderately obscured AGNs detected in X-rays, for which the X-ray-to-optical flux ratio (X/O)

is strongly correlated with the X-ray luminosity (Fiore et al. 2003; Eckart et al. 2006). The nuclear optical-UV light of these objects is completely blocked or strongly reduced by dust extinction, and the optical flux is dominated by the host galaxy. On the other hand, the 2–10 keV flux is reduced by only small factors, even for obscuring gas column densities of the order of a few  $\times 10^{23}\ \text{cm}^{-2}$ . Therefore, X/O is a good estimator of the ratio between the nuclear flux and the host galaxy starlight flux. While the nuclear AGN X-ray luminosity can span several decades, the host galaxy  $R$ -band luminosity has a moderate scatter, less than one decade, giving rise to the observed correlation between X/O and X-ray luminosity. Perola et al. (2004), Mignoli et al. (2004), Brusa et al. (2005), and Cocchia et al. (2007) found that the high-X/O sources tend to also be obscured in the X-rays, with column densities of the order of  $10^{22}$ – $10^{23}\ \text{cm}^{-2}$ . It is therefore possible to conclude that a high X/O ratio is a good indicator for both optical and moderate X-ray obscuration in high-luminosity sources. Interestingly, the  $F(24\ \mu\text{m})/F(R)$  of X-ray-selected sources is strongly correlated with X/O (Fig. 2, *right*). This suggests that luminous Compton-thick AGNs, which are faint in X-rays because of the strong photoelectric absorption and Compton scattering and cannot be selected using their X/O flux ratio, can be recovered using the  $F(24\ \mu\text{m})/F(R)$  ratio.

Furthermore, since X-ray-obscured AGNs tend to have red  $R-K$  colors (Brusa et al. 2005 and reference therein), one would also expect that Compton-thick AGNs have similarly red colors. Indeed, Figure 3 shows that the  $F(24\ \mu\text{m})/F(R)$  of X-ray-selected, obscured AGNs is correlated with the  $R-K$  color, as expected. Figure 3 also shows the isodensity contours of all the GOODS-MUSIC  $24\ \mu\text{m}$  sources with  $F(24\ \mu\text{m}) > 40\ \mu\text{Jy}$ . Intriguingly, the isodensity contours become narrow in  $F(24\ \mu\text{m})/F(R)$  at high  $R-K$  values and extend toward the region occupied by obscured X-ray-selected AGNs at high  $F(24\ \mu\text{m})/F(R)$  and high  $R-K$  values. The bimodality at high values of  $F(24\ \mu\text{m})/F(R)$  of the color distribution of the  $24\ \mu\text{m}$ -selected sources is evident in Figure 3 (*right*), which shows the fraction of GOODS-MUSIC  $24\ \mu\text{m}$  sources as a function of the  $R-K$  color in three

<sup>7</sup>  $F(24\ \mu\text{m})/F(R)$ ;  $\log F(R) = -0.4R - 22.5467$ .  $R$  magnitudes have been obtained by interpolating the  $V$  and  $I$  magnitudes in the GOODS-MUSIC catalog provided by *HST* ACS.

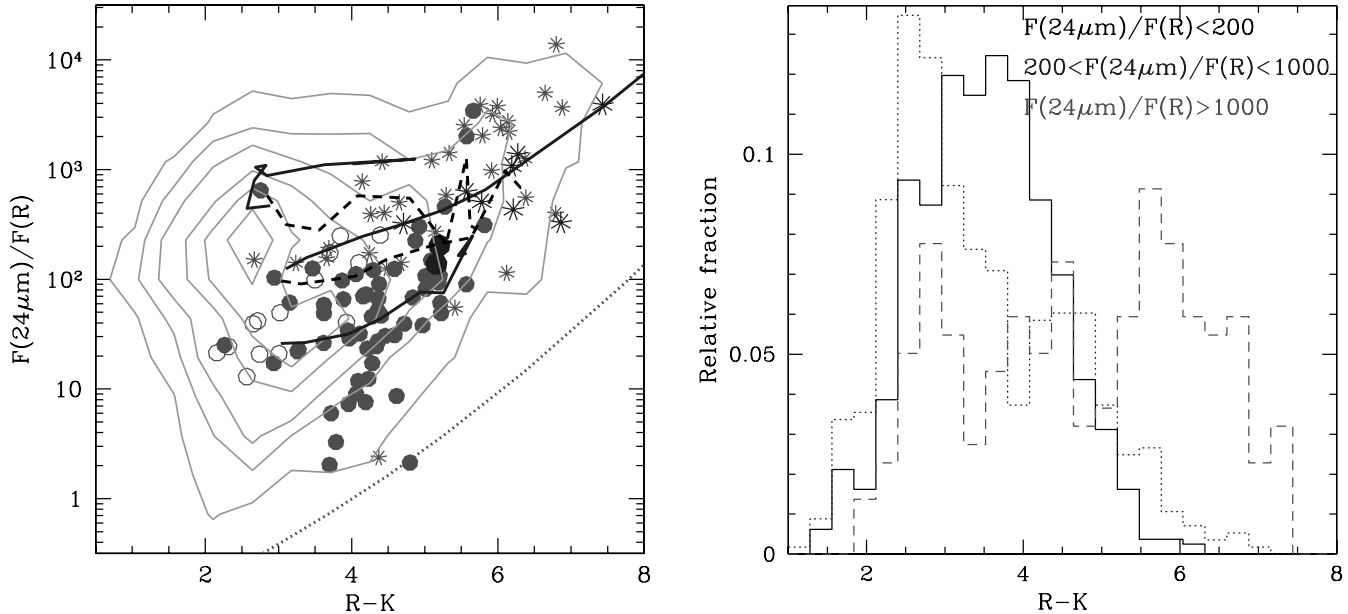


FIG. 3.—*Left:*  $F(24\ \mu\text{m})/F(R)$  as a function of  $R-K$  color for two X-ray source samples (GOODS-MUSIC and HELLAS2XMM, *large symbols*; Pozzi et al. 2007). Open circles are type 1 AGNs, filled circles are non-type 1 AGNs, and asterisks are photometric redshifts. Isodensity contours of all GOODS-MUSIC  $24\ \mu\text{m}$  sources are overlaid. The thick solid lines mark the expectations of three obscured AGN SEDs with redshift increasing from 0 to 4 (*left to right*). The lower curve represents the colors of a typical low-luminosity Seyfert 2 galaxy, the middle curve represents the colors of an obscured AGN from the Pozzi et al. sample (A2690\_75), and the upper curve represents the colors of IRAS 09104+41091. The black dashed lines are the expectations of the SEDs of two starburst galaxies (M82, *lower curve*; Arp 220, *upper curve*) for  $z = 0-4$ . The dotted line is the expectation of a passive elliptical galaxy for  $z = 0-4$ . *Right:* Fraction of GOODS-MUSIC  $24\ \mu\text{m}$  sources as a function of  $R-K$  color in three  $F(24\ \mu\text{m})/F(R)$  bins. The solid histogram represents  $F(24\ \mu\text{m})/F(R) < 200$ , the dotted histogram represents  $200 < F(24\ \mu\text{m})/F(R) < 1000$ , and the dashed histogram represents  $F(24\ \mu\text{m})/F(R) > 1000$ . [See the electronic edition of the Journal for a color version of this figure.]

$F(24\ \mu\text{m})/F(R)$  bins. While at low and intermediate  $F(24\ \mu\text{m})/F(R)$  values the distributions are peaked at  $R-K \sim 2.5-3.5$  and decrease smoothly toward higher  $R-K$  values, the distribution of the sources with  $F(24\ \mu\text{m})/F(R) > 1000$  shows a strong excess at  $R-K > 4.5$ .

It is interesting to note that most of the highly obscured AGNs selected in the HELLAS2XMM survey on the basis of their high X/O flux ratio (Pozzi et al. 2007) have  $F(24\ \mu\text{m})/F(R)$  higher than a few hundred, and all have  $R-K > 4.5$ . Their SEDs are characterized by a passive early-type galaxy in the optical and near-infrared and by an AGN component in the mid-infrared. These SEDs redshifted up to  $z = 4$  are able to explain the extreme colors of the  $F(24\ \mu\text{m})/F(R) > 1000$  and  $R-K > 4.5$  sources, unlike the SEDs of even extreme star-forming galaxies like Arp 220 (see Fig. 3, *left*). This strongly suggests that most of the  $F(24\ \mu\text{m})/F(R) > 1000$  and  $R-K > 4.5$  sources are powered by an active nucleus. Similar conclusions are found analyzing slightly different color diagrams, like  $F(24\ \mu\text{m})/F(R)$  versus  $F(24\ \mu\text{m})/F(8\ \mu\text{m})$  and  $F(24\ \mu\text{m})/F(R)$  versus  $F(3.6\ \mu\text{m})/F(z)$ .

### 3. X-RAY PROPERTIES OF EXTREME $24\ \mu\text{m}$ -SELECTED SOURCES

Our candidate obscured AGNs are selected from the full  $24\ \mu\text{m}$  GOODS-MUSIC sample with the criteria of having  $F(24\ \mu\text{m})/F(R) > 1000$  and  $R-K > 4.5$ . There are 135 such sources.

#### 3.1. Sources with a Direct X-Ray Detection

Eighteen of the 135 sources have an X-ray detection in Alexander et al. (2003). Four other sources are not formally detected but have more than 4–5 counts (after background subtraction) at the position of the  $24\ \mu\text{m}$  source. In summary, 22 of the 135 sources (16%) have a significant X-ray emission directly visible in the *Chandra* images.

Three of these 22 sources have a spectroscopic redshift with narrow-line optical spectra, and the other 19 have a photometric redshift in the GOODS-MUSIC catalog (see § 2); the median redshift and its interquartile range of these 22 sources is 2.1 (0.5) (interquartile ranges are indicated in parentheses after the median values).

The median monochromatic infrared luminosity at  $5.8\ \mu\text{m}$  is  $44.42\ (0.37)$ . The X-ray luminosities are in all cases higher than  $10^{42}\ \text{ergs s}^{-1}$ , making them bona fide AGNs. The median logarithmic ratio between the  $5.8\ \mu\text{m}$  and 2–10 keV luminosities is 1.07 (0.32). As a comparison, the median of the same logarithmic ratio for the full GOODS-MUSIC X-ray sample (150 AGNs with measured redshift) is 0.69 (0.47). The probability that the two distributions are drawn from the same parent population is 0.2%, using the Kolmogorov-Smirnov test.

The hardness ratios indicate in most cases a hard, possibly obscured X-ray spectrum. Indeed, these sources are among the most obscured ones in the Tozzi et al. (2006) analysis, all having column densities higher than a few  $\times 10^{22}\ \text{cm}^{-2}$  and two having column densities as high as  $10^{24}\ \text{cm}^{-2}$ .

Table 1 gives the breakdown of the best-fitting templates (see § 2) to the SEDs of these 22 sources. Fifteen SEDs are best fitted by one of the templates in Figure 1.

#### 3.2. Sources without a Direct X-Ray Detection

The total number of sources with  $F(24\ \mu\text{m})/F(R) > 1000$  and  $R-K > 4.5$  and no direct X-ray detection is 111 (we excluded two sources which happen to lie within  $5''$  of an X-ray source).

Four of these sources have a spectroscopic redshift, and 99 have a photometric redshift in the GOODS-MUSIC catalog. For four sources we could only compute a lower limit to the redshift. In conclusion, we have redshifts or limits for 107 sources. Both median redshift and infrared luminosity are similar to those of the 22 sources with a direct X-ray detection.

TABLE 1  
 TEMPLATE FITS TO THE SEDs OF THE SOURCES WITH  $F(24\ \mu\text{m})/F(R) > 1000$   
 AND  $R - K > 4.5$

Template	X-Ray Det.	Not X-Ray Det.
Ellipticals + S0 .....	...	2
Spirals.....	...	1
M82 + N6090 + Arp 220.....	...	35
I19254 + Mrk 231 .....	4	17
Seyfert 1.8–2 + red QSO.....	1	5
A2690_75 + BPM 16274_69.....	5	34
IRAS 09104+4109.....	9	11
N6240.....	1	1
Seyfert 1 + QSOs.....	2	1
Total.....	22	107

The redshift and infrared luminosity distributions of the  $F(24\ \mu\text{m})/F(R) > 1000$  and  $R - K > 4.5$  sources are compared in Figure 4 to those of the full GOODS-MUSIC  $24\ \mu\text{m}$  and X-ray-selected samples. The  $F(24\ \mu\text{m})/F(R) > 1000$  and  $R - K > 4.5$  sources have a redshift distribution with a median redshift of 1.91 (0.30). Excluding the lower limits,  $\langle z \rangle = 1.9$  (0.28). This distribution is shifted toward higher redshifts than both the full GOODS-MUSIC  $24\ \mu\text{m}$  source sample and the X-ray-selected AGN sample (Fig. 4, *left*). The right panel of Figure 4 shows that moderately obscured, X-ray-selected sources are concentrated below  $z = 1.5$  and span a range of infrared luminosities  $\log[\lambda L_\lambda(5.8\ \mu\text{m})] \sim 42\text{--}45.3$ . Their median 2–10 keV and infrared luminosities are 43.16 (0.56) and 43.84 (0.57), respectively. On the other hand, the  $F(24\ \mu\text{m})/F(R) > 1000$  and  $R - K > 4.5$  sources are concentrated between  $z = 1.2$  and 2.6 and have infrared luminosities from  $\log[\lambda L_\lambda(5.8\ \mu\text{m})] \sim 43.5$  to  $\sim 45.5$  with a median 44.34 (0.30), luminosities similar to those of the X-ray-selected AGNs at the same redshift.

Table 1 gives the results of the template fits to the observed SEDs of the 107 sources with a redshift. In 65% of the cases AGN templates provide the best fit. The majority of these SEDs are best fitted by one of the templates in Figure 1; the others are best fitted by one of the AGN templates of Polletta et al. (2007). Only one SED is best fitted by the template of a type 1 AGN. Thirty-six SEDs are best fitted by star-forming galaxy templates (in 30 cases the best fit is obtained using powerful star-forming galaxy templates, like those of Arp 220 and NGC 6090). In conclusion, the results of the SED fitting analysis confirm that the majority of the sources with  $F(24\ \mu\text{m})/F(R) > 1000$  and  $R - K > 4.5$  may be highly obscured AGNs. However, we remark that the results of the template fitting should not always be considered a quantitative determination of the nature of each single source, since in many cases different templates can produce fits with similar  $\chi^2$  in the observed optical–to– $24\ \mu\text{m}$  band, producing a degeneracy difficult to account for. Therefore, the results of the template fittings should only be taken as a qualitative indication of the population properties of the samples.

### 3.3. X-Ray Stacking Analysis

To validate our highly obscured AGN selection sample and assess quantitatively the fraction of bona fide AGNs in the  $F(24\ \mu\text{m})/F(R) > 1000$  and  $R - K > 4.5$  sample, we performed a detailed “stacking” analysis of the X-ray data of the  $24\ \mu\text{m}$ –selected sources. Indeed, thanks to the low *Chandra* background, it is possible to increase the effective exposure time and derive average properties of undetected objects using these stacking techniques: counts at the positions of known sources are co-added in

order to probe X-ray emission substantially below the single source sensitivity limit.

We performed a stacking analysis of the 111 sources not directly detected in the *Chandra* 1 Ms X-ray image. As control samples we used the 22 sources with  $F(24\ \mu\text{m})/F(R) > 1000$  and  $R - K > 4.5$  and an X-ray counterpart, a sample of sources with  $F(24\ \mu\text{m})/F(R) > 1000$  and  $R - K < 3.5$  (51 sources after the exclusion of the sources directly detected in the X-ray image), and a sample of sources with  $F(24\ \mu\text{m})/F(R) < 200$  and  $R - K > 4.5$  (73 sources after the exclusion of the sources directly detected in the X-ray image). The total exposure times for the four source samples are 94, 19.5, 43, and 61 Ms, respectively.

The top panels of Figure 5 (*left*) show the X-ray stack of the 111  $24\ \mu\text{m}$  sources with  $F(24\ \mu\text{m})/F(R) > 1000$  and  $R - K > 4.5$  in two energy bands. This is compared to the stack of 73 sources with  $F(24\ \mu\text{m})/F(R) < 200$  and  $R - K > 4.5$  and no direct X-ray detections (*bottom panels*). We choose bands 0.3–1.5 keV (soft band, S) and 1.5–4 keV (hard band, H) to keep the level of the internal background as low as possible and similar in the two bands. At a typical redshift of 2, these bands correspond to rest-frame energies of 0.9–4.5 and 4.5–12 keV, respectively. The stack of the high  $F(24\ \mu\text{m})/F(R)$  and high  $R - K$  sources produces a detection in both soft and hard bands, with count rates  $(0.98 \pm 0.20) \times 10^{-6}$  and  $(1.25 \pm 0.26) \times 10^{-6}$  counts  $\text{s}^{-1}$  in the two bands, respectively (using a  $2''$  radius extraction region). The hardness ratio  $H - S/H + S$  measured for this sample is therefore  $0.12 \pm 0.15$ . Conversely, no detection in either band is obtained for the stack of 51 sources with high  $F(24\ \mu\text{m})/F(R)$  and low  $R - K$ , with  $1\ \sigma$  upper limits of  $\sim 2 \times 10^{-7}$  counts  $\text{s}^{-1}$ . The stack of the low  $F(24\ \mu\text{m})/F(R)$  and high  $R - K$  sources produces a significant detection only in the soft band, with count rate  $(1.89 \pm 0.32) \times 10^{-6}$  counts  $\text{s}^{-1}$ . The count rate measured in the hard band is significant at less than  $3\ \sigma$  and corresponds to  $(4.9 \pm 1.9) \times 10^{-7}$  counts  $\text{s}^{-1}$ . The corresponding hardness ratio is  $H - S/H + S = -0.58 \pm 0.18$ . The stack of the 22 sources with  $F(24\ \mu\text{m})/F(R) > 1000$  and  $R - K > 4.5$  and an X-ray counterpart produces a hardness ratio  $H - S/H + S = -0.06 \pm 0.01$ . In conclusion, the stack of the 111 sources with  $F(24\ \mu\text{m})/F(R) > 1000$  and  $R - K > 4.5$  and without a direct X-ray detection produces a significant signal in both soft and hard X-ray bands. It is interesting to note that its hardness ratio suggests an average spectrum harder than even the average spectrum of the 22 sources with similar infrared and optical colors but with a direct X-ray detection.

### 3.4. Simulations to Assess the Fraction of Obscured AGNs in the $24\ \mu\text{m}$ Source Samples

We used the observed flux in the stacked images, together with the hardness ratio  $H - S/H + S$ , to constrain the fraction of highly obscured AGNs in the samples. To this purpose, we generated simulated X-ray count rates and hardness ratios as a function of the fraction of the AGNs, assuming that the  $F(24\ \mu\text{m})/F(R) > 1000$  and  $R - K > 4.5$  source sample is made by obscured AGNs and star-forming galaxies. We started from the observed redshift and infrared luminosities, and for the obscured AGNs we assumed a  $\log[\lambda L_\lambda(5.8\ \mu\text{m})/L(2\text{--}10\ \text{keV})]$  luminosity ratio chosen randomly in the range 0.4–1.2. The lower value is the typical ratio found by Silva et al. (2004) for low-luminosity Seyfert 2 galaxies with column density  $\log N_{\text{H}} \lesssim 24$ . It is also similar to the ratio found for the two HELLAS2XMM sources A2690\_75 and BPM 16274\_69. The upper value is the ratio found for the powerful obscured QSO IRAS 09104+4109 (Piconcelli et al. 2007).

For the star-forming galaxies we used a  $\log[\lambda L_\lambda(5.8\ \mu\text{m})/L(2\text{--}10\ \text{keV})]$  luminosity ratio between 2 and 2.8. These two

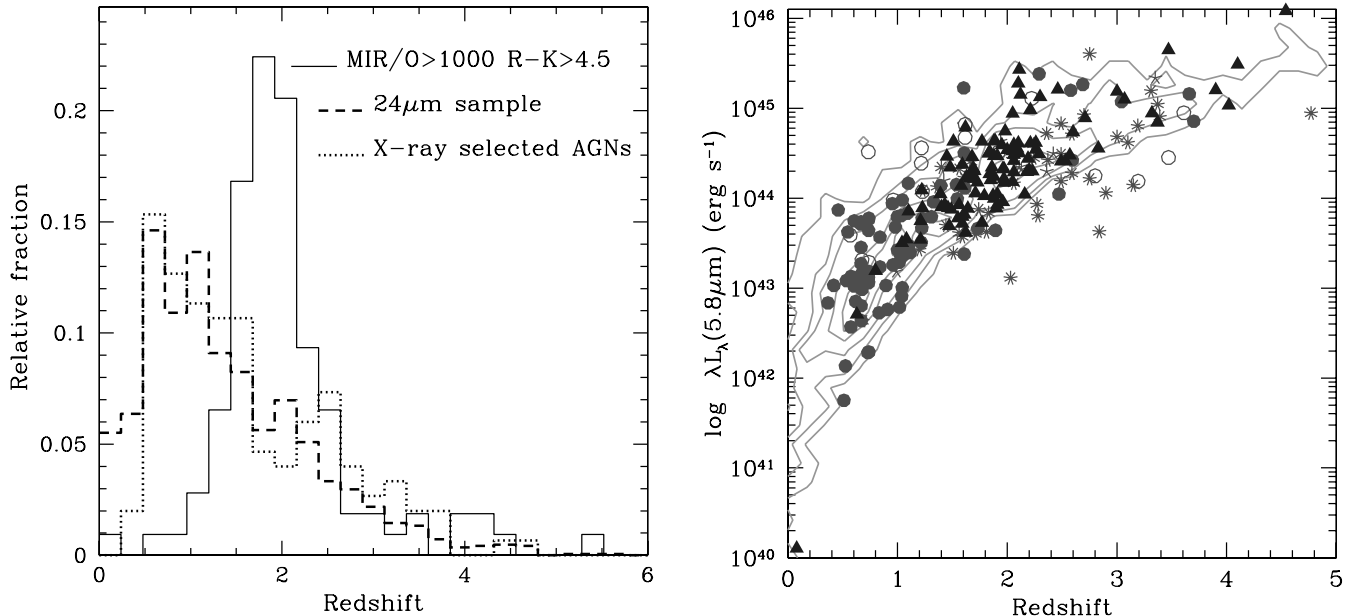


FIG. 4.—*Left*: Redshift distribution of the  $F(24\ \mu\text{m})/F(R) > 1000$  and  $R - K > 4.5$  sources without direct X-ray detection (107 sources) compared to those of the full GOODS-MUSIC  $24\ \mu\text{m}$  sample (1649 sources) and the X-ray-selected AGNs in the GOODS-MUSIC area (150 sources). *Right*: Redshift-infrared luminosity ( $\log[\lambda_{L_{\lambda}}(5.8\ \mu\text{m})]$ ) plane for the full  $24\ \mu\text{m}$  GOODS-MUSIC source sample (isodensity contours), the CDFS X-ray AGN sample (open circles are type 1 AGNs, filled circles are non-type 1 AGNs, and asterisks are photometric redshifts), and the sample of  $F(24\ \mu\text{m})/F(R) > 1000$  and  $R - K > 4.5$  sources without direct X-ray detection (triangles). [See the electronic edition of the Journal for a color version of this figure.]

values are obtained assuming a total infrared to 2–10 keV logarithmic luminosity ratio of 3.6 (Ranalli et al. 2003) and correcting this for the ratio of the total infrared luminosity and the  $5.8\ \mu\text{m}$  luminosity of powerful star-forming galaxies and spiral templates.

We further assumed that the star-forming galaxies are not obscured in X-rays, while the AGNs are highly obscured. For the latter objects, we adopted a flat  $\log N_{\text{H}}$  distribution from  $23$  to  $26\ \text{cm}^{-2}$ .

For a given fraction of AGNs in the sample, we first decided, using a random generator, whether each source was an AGN or a star-forming galaxy. Then, if the source turned out to be an AGN, we chose an absorbing column density, again using a random generator and the assumed  $\log N_{\text{H}}$  distribution. We computed unobscured 2–10 keV luminosities from infrared luminosities and then X-ray fluxes by folding a power-law spectrum with a spectral energy index of 0.8 reduced at low energy by photoelectric absorption with a *Chandra* response matrix. For column densities of  $10^{25}\ \text{cm}^{-2}$  we assumed that the direct emission was completely blocked by photoelectric absorption and Compton scattering. For these sources we assumed a reflection component with a normalization of 1/100 of the direct component and the same spectral index.

A small fraction of the simulated count rates (20%–30%) is higher than the *Chandra* detection limit. This was expected, given the fact that 22 out of 135 sources with  $F(24\ \mu\text{m})/F(R) > 1000$  and  $R - K > 4.5$  do have X-ray counterparts. Since we are interested in the fraction of AGNs in the sources not directly detected in the *Chandra* images, these count rates have been excluded from the following analysis.

The result of the simulations is shown in Figure 5 (*right*). According to our simulations, the average hardness ratio of the  $F(24\ \mu\text{m})/F(R) > 1000$  and  $R - K > 4.5$  source sample without X-ray detection is reproduced if  $80\% \pm 15\%$  of the sources in the sample are highly obscured AGNs. The hardness ratio of the sources with  $F(24\ \mu\text{m})/F(R) < 200$  and  $R - K > 4.5$  is

reproduced if the fraction of the obscured AGNs is in the range 0%–20%. Changing the assumptions made to produce the simulations within reasonable ranges changes this result only slightly.

The result of the simulations concerning the  $F(24\ \mu\text{m})/F(R) > 1000$  and  $R - K > 4.5$  source sample is quite consistent with the indications from the 1– $24\ \mu\text{m}$  SED fitting with galaxy and AGN templates presented in the previous section.

#### 4. DISCUSSION AND CONCLUSIONS

We selected a source sample with an extreme mid-infrared–to–optical flux ratio [ $F(24\ \mu\text{m})/F(R) > 1000$ ] and red optical colors ( $R - K > 4.5$ ) in the GOODS CDFS area. These sources are among the most luminous sources in the GOODS  $24\ \mu\text{m}$  sample, because of the correlation of  $F(24\ \mu\text{m})/F(R)$  with the infrared luminosity (see Figs. 2 and 4, *right*). The fraction of these sources not directly detected in the *Chandra* images produces a significant stacked signal in both *Chandra* soft and hard X-ray bands. A detailed analysis based on Monte Carlo simulations shows that the stacked count rates and hardness ratios can be reproduced if this source population is dominated by highly obscured ( $N_{\text{H}} > \text{a few} \times 10^{23}\ \text{cm}^{-2}$ ) AGNs.

This conclusion is further confirmed by the following consideration. If we assume that this source population is dominated by star-forming galaxies, we can use the observed infrared luminosity and the dust-corrected UV luminosities to derive two different estimates of star formation rates. On one hand, total infrared luminosities have been converted to a star formation rate using the following formula:  $\text{SFR} = L_{\text{IR}}/(2.24 \times 10^{43}\ \text{ergs s}^{-1}) M_{\odot}\ \text{yr}^{-1}$  (Kennicutt 1998). On the other hand, the UV star formation rate is an output of the fits of the observed SEDs with synthetic models. These models have been obtained using the Bruzual & Charlot (2003) models, parameterizing the star formation histories with a variety of exponentially declining laws (with timescales ranging from 0.1 to 15 Gyr) and metallicities (from  $Z = 0.02$  to 2.5; see Grazian et al. 2006 and references therein for further details). Dust extinction is added to all star-forming models with

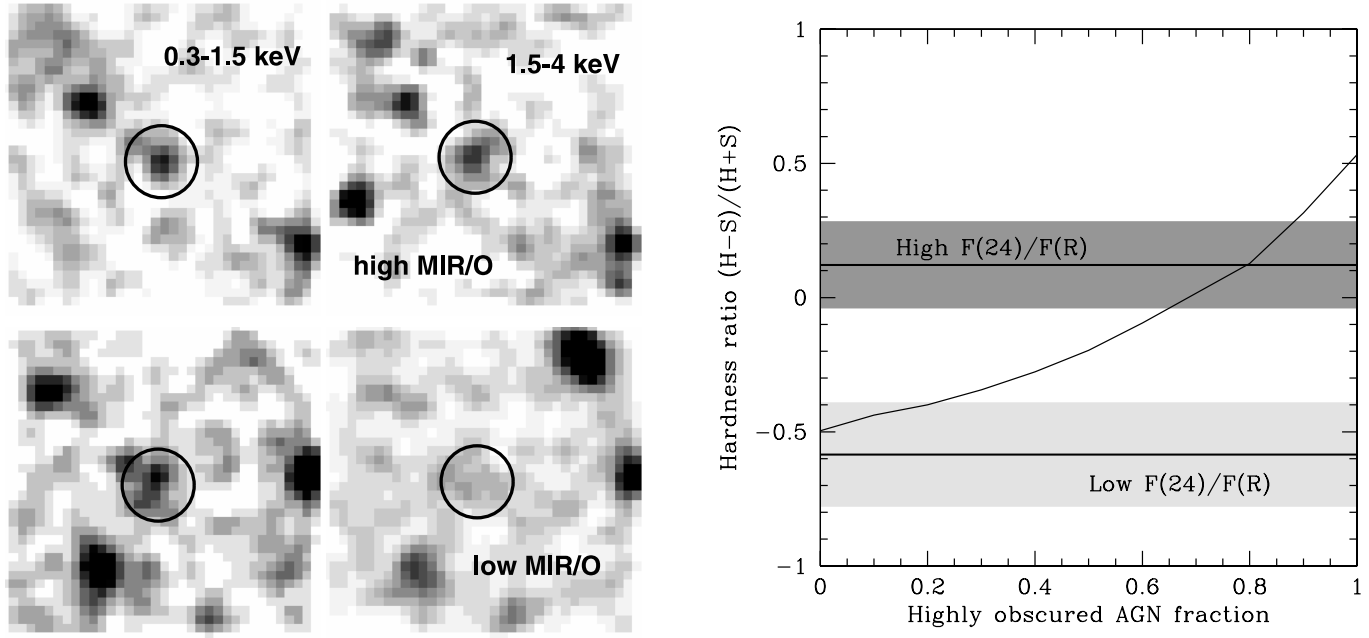


FIG. 5.—*Left*: Stacked X-ray images of  $24\ \mu\text{m}$  GOODS-MUSIC sources. The images have sides of  $18''$ , and the central circles have  $2''$  radii. The top panels refer to 111 sources with  $F(24\ \mu\text{m})/F(R) > 1000$  and  $R - K > 4.5$ ; the bottom panels refer to 73 sources with  $F(24\ \mu\text{m})/F(R) < 200$  and  $R - K > 4.5$ . The left panels are stacks in the soft 0.3–1.5 keV band, and the right panels are stacks in the hard 1.5–4 keV band. *Right*: Hardness ratio  $(H-S)/(H+S)$  of the counts in circles of  $2''$  radii as a function of the fraction of highly obscured AGNs for the sample of 111  $24\ \mu\text{m}$  GOODS-MUSIC sources with  $F(24\ \mu\text{m})/F(R) > 1000$  and  $R - K > 4.5$ . The solid curve is the result of Monte Carlo simulations (see text for details); the two horizontal lines are the average hardness ratios measured for the  $F(24\ \mu\text{m})/F(R) > 1000$  and  $R - K > 4.5$  (*upper line*) and the  $F(24\ \mu\text{m})/F(R) < 200$  and  $R - K > 4.5$  sources (*lower line*). The shaded bands mark the hardness ratio statistical uncertainties. [See the electronic edition of the *Journal* for a color version of this figure.]

$0 < E(B - V) < 1.1$  and a Calzetti attenuation curve. Given the very red colors of our objects in the optical bands, they are typically fit with star-forming templates with a large dust extinction [ $E(B - V) > 0.5$ ], resulting in a star formation rate much larger than that derived by a simple, dust-free UV-to-SFR conversion.

The median logarithmic star formation rate from infrared luminosity is  $2.31\ (0.59)\ M_{\odot}\ \text{yr}^{-1}$ . The median logarithmic UV star formation rate is  $0.83\ (0.80)\ M_{\odot}\ \text{yr}^{-1}$ , a factor of 30 lower. The large mismatch between these two estimates strongly suggests that the infrared luminosity of this source sample is not dominated by star formation but rather by accretion. As a comparison, the median infrared and UV star formation rates of the sources with  $F(24\ \mu\text{m})/F(R) < 200$  and  $R - K > 4.5$  in our control sample are  $1.26\ (0.38)$  and  $1.10\ (0.30)$ , respectively, consistent with each other, suggesting that the infrared luminosity of these sources is not dominated by nuclear accretion (in agreement with their X-ray hardness ratio; see previous section).

We can now compare the number of highly obscured AGNs selected at  $24\ \mu\text{m}$  and not detected in X-rays with the number of unobscured and moderately obscured AGNs directly seen in the X-ray images. To reduce the importance of complex selection effects we limit this analysis to the sources in the redshift bin  $1.2-2.6$ . At  $z = 2.6$  the  $5.8\ \mu\text{m}$  luminosity corresponding to the limit of  $40\ \mu\text{Jy}$  at  $24\ \mu\text{m}$  is  $\log[\lambda L_{\lambda}(5.8\ \mu\text{m})] = 44.3-44.2$  for Seyfert 2 and 1.8 galaxy SEDs and  $44.4-44.5$  for the four SEDs in Figure 1. Assuming a  $\log[\lambda L_{\lambda}(5.8\ \mu\text{m})/L(2-10\ \text{keV})]$  luminosity ratio in the range  $0.4-1.2$  implies unobscured 2–10 keV luminosities in the range  $43.3-43.9$ . This suggests limiting the comparison to the sources with  $\log L(2-10\ \text{keV}) > 43$  and  $\log[\lambda L_{\lambda}(5.8\ \mu\text{m})] \gtrsim 44.2$ .

In the  $1.2-2.6$  redshift bin there are at least  $46 \pm 10$  sources with  $F(24\ \mu\text{m})/F(R) > 1000$ ,  $R - K > 4.5$ ,  $\log[\lambda L_{\lambda}(5.8\ \mu\text{m})] \gtrsim 44.2$ , and no direct X-ray detection ( $80\% \pm 15\%$  of 57 sources), which are probably highly obscured AGNs, and 44 X-ray-

selected AGNs, 7 of which have broad lines in their optical spectra. The number of  $24\ \mu\text{m}$ -selected, presumably highly obscured AGNs missed by the CDFS X-ray survey is therefore similar to the number of X-ray-selected AGNs.

The median  $5.8\ \mu\text{m}$  luminosity of the 57  $F(24\ \mu\text{m})/F(R) > 1000$  and  $R - K > 4.5$  sources without direct X-ray detection in the redshift and luminosity bins defined above is  $\log[\lambda L_{\lambda}(5.8\ \mu\text{m})] = 44.48\ (0.30)$ , implying a median unobscured 2–10 keV luminosity in the range  $43.3-44.1$ , adopting our assumption on the infrared-to-X-ray flux ratio. At  $z = 2.6$  these luminosities translate to X-ray fluxes between a few times  $10^{-16}$  and  $10^{-14}\ \text{ergs cm}^{-2}\ \text{s}^{-1}$ , meaning that these sources would have been easily detected if they were not highly obscured.

We have compared our findings with the predictions of the La Franca et al. (2005) and Gilli et al. (2007) models. In the redshift bin  $1.2-2.6$  and in the area covered by our  $24\ \mu\text{m}$  sample the La Franca et al. (2005) luminosity function predicts about 75 AGNs with  $\log L(2-10\ \text{keV}) > 43$ , 20 of which have a column density of  $10^{24}\ \text{cm}^{-2}$ . The absorption distribution adopted by the Gilli et al. (2007) AGN synthesis model for the cosmic X-ray background predicts about 40 Compton-thick AGNs with the same limits for redshift and luminosity. We find  $46 \pm 10$   $24\ \mu\text{m}$ -selected, highly obscured AGNs, a number about twice the La Franca et al. (2005) prediction but quite consistent with the Gilli et al. (2007) prediction.

Marconi et al. (2004) derived a SMBH mass function from the X-ray-selected AGN luminosity functions that falls short by a factor of about 2 of the “relic” SMBH mass function. This difference can be greatly alleviated by adding the population of infrared-selected, highly obscured AGNs to the AGNs selected in the X-ray band below 10 keV.

Finally, we note that the population of infrared-selected, highly obscured AGNs can help in reconciling the predictions of models of galaxy evolution with the observed AGN number

densities at  $z \gtrsim 1-1.5$ . Indeed, the Menci et al. (2004) model predicts a number of low-to-intermediate luminosity AGNs at  $z = 1.5-2.5$ , about twice that measured through X-ray 2–10 keV surveys (La Franca et al. 2005; Fiore 2006). We found above that in the redshift bin 1.2–2.6 the number of X-ray-selected AGNs with  $\log L(2-10 \text{ keV}) > 43$  is comparable to that of the infrared-selected, highly obscured AGNs. Therefore, adding together the two populations would give a total number density of AGNs similar to that predicted by the Menci et al. (2004) model. More detailed, quantitative AGN number density calculations, spanning wider redshift and luminosity ranges, are beyond the purpose of this paper and will be presented elsewhere (F. Fiore et al. 2008, in preparation).

Most of the GOODS-MUSIC 24  $\mu\text{m}$ -selected sources with high  $F(24 \mu\text{m})/F(R)$ , high  $R - K$ , and no X-ray detection have a very faint optical and near-infrared counterpart, with only 14% of the sample having  $R \lesssim 26$ . Furthermore, only a handful of objects have a mid-infrared flux high enough [ $F(24 \mu\text{m}) \gtrsim 0.5 \text{ mJy}$ ] to allow *Spitzer* IRS spectroscopy. The spectroscopic identification of  $\sim 90\%$  of the sample must therefore await the advent of extremely large telescopes or the launch of the *James Webb Space Telescope*.

Our analysis is limited to AGNs of intermediate luminosity at  $z \sim 2$ . To extend the coverage of the luminosity-redshift plane requires a complementary observation strategy. Particularly useful to this purpose is the SWIRE survey, which has both *Spitzer*

and optical medium-deep coverage on  $\sim 50 \text{ deg}^2$  of sky. As an example, the SWIRE survey contains hundreds of sources with extreme  $F(24 \mu\text{m})/F(R)$  flux ratios and red optical/near-infrared colors. Interestingly, several dozen of these extreme sources have 24  $\mu\text{m}$  flux higher than  $\sim 1 \text{ mJy}$ , allowing *Spitzer* IRS spectroscopy, and/or optical magnitude brighter than  $R \sim 25$ , allowing spectroscopy with 8 m class telescopes. Furthermore, all these sources are well within the reach of Herschel instruments between 75 and 500  $\mu\text{m}$ . Such long-wavelength observations can greatly help in separating nuclear activity from star formation when the two components have comparable integrated luminosities, e.g., in low-luminosity, Seyfert-like AGNs.

We are grateful to Fabio La Franca and Roberto Maiolino for useful discussions. We thank an anonymous referee for comments that helped improve the presentation. After submission of this paper to ApJ we became aware of a work by a different group reaching similar conclusions (Daddi et al. 2007). We thank Emanuele Daddi for providing a copy of his manuscript before submission and for useful discussions. Part of this work was supported by ASI/INAF contracts I/023/05/0 and I/024/05/0 and by PRIN/MUR grant 2006-02-5203. Part of this work was supported by the Deutsches Zentrum für Luft- und Raumfahrt, DLR project numbers 50 OR 0207 and 50 OR 0405.

## REFERENCES

- Alexander, D. M., et al. 2003, AJ, 126, 539  
 Alonso-Herrero, A., et al. 2006, ApJ, 640, 167  
 Barnby, P., et al. 2006, ApJ, 642, 126  
 Bongiorno, A., et al. 2007, A&A, 472, 443  
 Brandt, W. N., & Hasinger, G. 2005, ARA&A, 43, 827  
 Brusa, M., et al. 2005, A&A, 432, 69  
 Bruzual, G., & Charlot, S. 2003, MNRAS, 344, 1000  
 Cavaliere, A., & Vittorini, V. 2000, ApJ, 543, 599  
 Cimatti, A., et al. 2002, A&A, 381, L68  
 Cocchia, F., et al. 2007, A&A, 466, 31  
 Coleman, G. D., Wu, C.-C., & Weedman, D. W. 1980, ApJS, 43, 393  
 Comastri, A. 2004, in Supermassive Black Holes in the Distant Universe, ed. A. J. Barger (Dordrecht: Kluwer), 245  
 Cowie, L. L., Songaila, A., Hu, E. M., & Cohen, J. G. 1996, AJ, 112, 839  
 Daddi, E., et al. 2007, ApJ, 670, 173  
 De Lucia, G., Springel, V., White, S. D. M., Croton, D., & Kauffmann, G. 2006, MNRAS, 366, 499  
 De Santis, C., Grazian, A., Fontana, A., & Santini, P. 2007, NewA, 12, 271  
 Di Matteo, T., Springel, V., & Hernquist, L. 2005, Nature, 433, 604  
 Eckart, M. E., Stern, D., Helfand, D., Harrison, F. A., Mao, P. H., & Yost, S. A. 2006, ApJS, 165, 19  
 Fabian, A. C. 1999, MNRAS, 308, L39  
 Ferrarese, L., & Merritt, D. 2000, ApJ, 539, L9  
 Fioc, M., & Rocca-Volmerange, B. 1997, A&A, 326, 950  
 Fiore, F. 2006, Mem. Soc. Astron. Italiana, 77, 694  
 Fiore, F., et al. 2003, A&A, 409, 79  
 Franceschini, A., Hasinger, G., Miyaji, T., & Malguori, D. 1999, MNRAS, 310, L5  
 Gebhardt, K., et al. 2000, ApJ, 543, L5  
 Giacomini, R., et al. 2002, ApJS, 139, 369  
 Gilli, R., Comastri, A., & Hasinger, G. 2007, A&A, 463, 79  
 Gilli, R., Salvati, M., & Hasinger, G. 2001, A&A, 366, 407  
 Granato, G. L., De Zotti, G., Silva, L., Bressan, A., & Danese, L. 2004, ApJ, 600, 580  
 Granato, G. L., Silva, L., Monaco, P., Panuzzo, P., Salucci, P., De Zotti, G., & Danese, L. 2001, MNRAS, 324, 757  
 Grazian, A., et al. 2006, A&A, 449, 951  
 Hasinger, G. 2003, in AIP Conf. Proc. 666, The Emergence of Cosmic Structure, ed. S. S. Holt & C. S. Reynolds (Melville: AIP), 227  
 Hasinger, G., Miyaji, T., & Schmidt, M. 2005, A&A, 441, 417  
 Houck, J. R., et al. 2005, ApJ, 622, L105  
 Kennicutt, R. C., Jr. 1998, ARA&A, 36, 189  
 Lacy, M., et al. 2004, ApJS, 154, 166  
 La Franca, F., et al. 2005, ApJ, 635, 864  
 Le Fevre, O., et al. 2004, A&A, 428, 1043  
 Magliocchetti, M., Silva, L., Lapi, A., de Zotti, G., Granato, G. L., Fadda, D., & Danese, L. 2007, MNRAS, 375, 1121  
 Marconi, A., & Hunt, L. 2003, ApJ, 589, L21  
 Marconi, A., Risaliti, G., Gilli, R., Hunt, L. K., Maiolino, R., & Salvati, M. 2004, MNRAS, 351, 169  
 Martinez-Sansigre, A., Rawlings, S., Lacy, M., Fadda, D., Jarvis, M. J., Marleau, F. R., Simpson, C., & Willott, C. J. 2006, MNRAS, 370, 1479  
 Martinez-Sansigre, A., Rawlings, S., Lacy, M., Fadda, D., Marleau, F. R., Simpson, C., Willott, C. J., & Jarvis, M. J. 2005, Nature, 436, 666  
 Menci, N., Fiore, F., Perola, G. C., & Cavaliere, A. 2004, ApJ, 606, 58  
 Menci, N., Fontana, A., Giallongo, E., & Salimbeni, S. 2005, ApJ, 632, 49  
 Mignoli, M., et al. 2004, A&A, 418, 827  
 ———. 2005, A&A, 437, 883  
 Perola, G. C., et al. 2004, A&A, 421, 491  
 Piconcelli, E., Fiore, F., Nicastro, F., Mathur, S., Brusa, M., Comastri, A., & Puccetti, S. 2007, A&A, 473, 85  
 Polletta, M., et al. 2006, ApJ, 642, 673  
 ———. 2007, ApJ, 663, 81  
 Pozzi, F., et al. 2007, A&A, 468, 603  
 Ranalli, P., Comastri, A., & Setti, G. 2003, A&A, 399, 39  
 Silk, J., & Rees, M. J. 1998, A&A, 331, L1  
 Silva, L., Maiolino, R., & Granato, G. L. 2004, MNRAS, 355, 973  
 Soltan, A. 1982, MNRAS, 200, 115  
 Szokoly, G. P., et al. 2004, ApJS, 155, 271  
 Tozzi, P., et al. 2006, A&A, 451, 457  
 Ueda, Y., Akiyama, M., Ohta, K., & Miyaji, T. 2003, ApJ, 598, 886  
 Vanzella, E., et al. 2005, A&A, 434, 53  
 ———. 2006, A&A, 454, 423  
 Weedman, D. W., Le Floc'h, E., Higdon, S. J. U., Higdon, J. L., & Houck, J. R. 2006a, ApJ, 638, 613  
 Weedman, D. W., et al. 2006b, ApJ, 651, 101  
 Worsley, M. A., Fabian, A. C., Barcons, X., Mateos, S., Hasinger, G., & Brunner, H. 2004, MNRAS, 352, L28  
 Worsley, M. A., Fabian, A. C., Bauer, F. E., Alexander, D. M., Brandt, W. N., & Lehmer, B. D. 2006, MNRAS, 368, 1735  
 Yan, L., et al. 2007, ApJ, 658, 778